Published in final edited form as:
Inorg Chem. 2009 December 7; 48(23): 11038–11047. doi:10.1021/ic901391y.

Reactivities of Fe(IV) Complexes with Oxo, Hydroxo, and Alkylperoxo Ligands: An Experimental and Computational Study

Adam T. Fiedler and **Lawrence Que Jr.***
Contribution from the Department of Chemistry and the Center for Metals in Biocatalysis, University of Minnesota, 207 Pleasant St. SE, Minneapolis, Minnesota 55455

Abstract

In a previous paper (Jensen *et al.*, *J. Am. Chem. Soc.* **2005**, *127*, 10512), we reported the synthesis of the turquoise-colored intermediate $[Fe^{IV}(\beta\text{-BPMCN})(O O^{t}Bu)(OH)]^{2+}$ (**Tq**; BPMCN = *N*,*N*′-bis (2-pyridylmethyl)-*N*,*N*′-dimethyl-*trans*-1,2-diaminocyclohexane). The structure of **Tq** is unprecedented, as it represents the only synthetic example to date of a non-heme Fe^{IV} complex with both alkylperoxo and hydroxide ligands. Given the significance of similar high-valent Fe intermediates in the mechanisms of oxygenase enzymes, we have explored the reactivity of **Tq** at −70 °C, a temperature at which it is stable, and found that it is capable of activating weak X-H bonds (X = C, O) with bond dissociation energies ≤~80 kcal/mol. The Fe^{IV}-OH unit of **Tq**, and not the alkylperoxo moiety, performs the initial H-atom abstraction. However at −45 °C, **Tq** decays at a rate that is independent of substrate identity and concentration, forming a species capable of oxidizing substrates with stronger C-H bonds. Parallel reactivity studies were also conducted with the related oxoiron(IV) complexes $[Fe^{IV}(\beta\text{-BPMCN})(O)(X)]^{2+}$ (**3-X**; X = pyridine or nitrile), thereby permitting a direct comparison of the reactivity of Fe^{IV} centers with oxo and hydroxide ligands. We found that the H-atom abstracting ability of the Fe^{IV}=O species greatly exceeds that of the Fe^{IV}-OH species, generally by greater than 100-fold. Examination of the electronic structures of **Tq** and **3-X** with density functional theory (DFT) provides a rationale for their differing reactivities.

Introduction

Nature employs a number of heme and nonheme Fe-dependent enzymes to carry out the selective oxidation of H-X bonds (X = C, N, or O). Such enzymes typically require dioxygen to generate a reactive Fe-containing intermediate, which then abstracts a hydrogen-atom from substrate.[1,2] The active intermediates are often mononuclear Fe^{IV} species with terminal oxo ligands, such as compound I of cytochrome P450[3] and intermediate **J** of the α-ketoacid-dependent enzyme TauD.[4] Alternatively, the oxidant can be a high-valent diiron species with bridging oxo ligands, such as the putative $Fe^{IV}{}_2(\mu\text{-O})_2$ core of intermediate **Q** in methane monooxygenase (MMO) or the mixed-valent $Fe^{III}(\mu\text{-O})Fe^{IV}$ intermediate **X** of ribonucleotide reductase (RNR).[5] Finally, it has been proposed that Fe^{III}-OH and Fe^{III}-OOH species serve as the active oxidants in lipoxygenase[6] and bleomycin,[7] respectively, indicating that ferric intermediates are also viable oxidants.

CORRESPONDING AUTHOR: larryque@umn.edu.

Supporting Information Available: Detailed kinetic data for the reaction of **Tq** with TTBP (Figure S1) and various phenols (Figure S2). EPR and Resonance Raman spectra of product solutions generated by reaction of **Tq** with phenols (Figures S3 and S4, respectively). Absorption spectra of the reaction of **Tq** with DHA in CH_2Cl_2 (Figure S5) and the reaction of **3- NCR** with TTBP in PrCN (Figure S6). Detailed kinetic data for the reaction of **3-NCR** with TTBP (Figure S7). Absorption spectra for the reaction of **Tq** at −45°C with cyclohexene (Figure S8). Cartesian coordinates for the DFT geometry-optimized models $\mathbf{Tq}^{\mathbf{A}}$, $\mathbf{Tq}^{\mathbf{B}}$, $\mathbf{3}^{\mathbf{A}}$**-NCMe**, and $\mathbf{3}^{\mathbf{B}}$**-NCMe** (Table S1(a–d)). This material is available free of charge via the Internet at http://pubs.acs.org.

Each of the Fe intermediates described above contains an Fe/O unit that directly participates in the H-atom abstraction, as shown in the general equations 1–4:

$$Fe^{n+}=O+H-R \rightarrow Fe^{(n-1)+}-OH+R^{\bullet} \quad (1)$$

$$Fe^{n+}-OH+H-R \rightarrow Fe^{(n-1)+}-OH_2+R^{\bullet} \quad (2)$$

$$[Fe-O-Fe]^{n+}+H-R \rightarrow [Fe-O(H)-Fe]^{n+}+R^{\bullet} \quad (3)$$

$$Fe^{n+}-OOH+H-R \rightarrow Fe^{(n+1)+}=O+H_2O+R^{\bullet} \quad (4)$$

Given that such a wide variety of Fe intermediates are involved in H-X bond activation, it is crucial to identify the structural and electronic features that control their reactivity. A particularly important issue concerns the relative H-atom abstracting abilities of Fe^{IV}=O, Fe^{IV}-OH, and Fe^{IV}-O- M species (M = metal ion), as all three types of structures have been invoked in biological and synthetic systems. Of course, direct comparisons of such reactivities are greatly facilitated by the use of similar supporting ligand environments and reaction conditions, which is easiest to achieve with synthetic complexes. To this end, Busch and coworkers recently employed a series of $Mn^{IV}(OH)_x(O)_y$ complexes that are supported by the same tetradentate macrocyclic ligand to compare the H-atom abstracting abilities of Mn^{IV}-OH and Mn^{IV}=O units.[8,9] However, no study to date has explored the comparative reactivity of Fe^{IV} =O and Fe^{IV}–OH complexes, despite the fact that such species are relevant to a number of biological systems.

In 2005, we reported that treatment of [Fe^{II}(β-BPMCN)$(OTf)_2$] (**1,** BPMCN = *N*,*N*′-bis(2-pyridylmethyl)-*N*,*N*′-dimethyl-*trans*-1,2-diaminocyclohexane) with *tert*-butyl hydroperoxide (TBHP) yields two distinct iron(IV) complexes, depending upon solvent.[10] In both MeCN and CH_2Cl_2 solutions, the initial reaction results in formation of an Fe^{III}-OO^{t}Bu species (**2**; Scheme 1). In MeCN at −40 °C, **2-MeCN** slowly converts via O-O bond homolysis to the oxoiron(IV) complex [Fe^{IV}(β-BPMCN)(O)(NCMe)]$^{2+}$ (**3-MeCN**), which exhibits a pale green color. By contrast, in CH_2Cl_2 at −70 °C, the reaction gives rise to a complex with a *deep turquoise color*; detailed spectroscopic studies identified this species as [Fe^{IV}(β-BPMCN)(OO^{t}Bu)(OH)]$^{2+}$ (**Tq**; Scheme 1).[10] The structure of **Tq** is remarkable; it represents the only example to date of a well-characterized alkylperoxoiron(IV) complex, and one of only two isolable nonheme Fe^{IV}-OH compounds (the other example is [Fe^{IV}(O)(Me^4-cyclam)(OH)]$^{2+}$).[11] Furthermore, the chemistry shown in Scheme 1 is unique in that, *with the same supporting ligand*, we can generate metastable Fe^{IV} complexes with oxo, hydroxo, and alkylperoxo ligands.

Clearly, the Fe(β-BPMCN) framework provides an unprecedented opportunity to explore the role of ligand identity in modulating the oxidizing power of high-valent Fe centers. We have therefore sought to measure and compare the reactivities of complexes **Tq** and **3** towards various organic substrates. While the H-atom abstracting ability of Fe^{IV}=O complexes has been studied extensively,[12–15] there are no extant reports on the chemistry of nonheme Fe^{IV}-OH complexes. **Tq** is also interesting due to the fact that it possesses two reactive sites – the hydroxo and alkylperoxo ligands. Indeed, we will demonstrate below that both functionalities are capable of participating in the oxidation of substrates, depending upon reaction conditions. Our

results also indicate that the H-atom abstracting ability of the Fe^{IV}=O species (**3**) greatly exceeds that **Tq**. Examination of the electronic structures of these two Fe^{IV} complexes with computational methods provides a rationale for their differing reactivities.

Experimental Section

Materials and Synthesis

All reagents were purchased from commercial sources and used as received, unless noted otherwise. Butyronitrile (PrCN) was purified by heating over Na_2CO_3 and $KMnO_4$ for several hours, followed by distillation and drying over molecular sieves. MeCN and CH_2Cl_2 were purified by distillation from CaH_2. The β-BPMCN ligand and complex **1** were synthesized following literature procedures.[16] Prior to their use in reactivity studies, cyclohexene, styrene, 1,4-cyclohexadiene, and stilbene were purified by passage through basic alumina. 9,10-dihydroanthracene (DHA) and 2,4,6-tri-*tert*-butylphenol (TTBP) were both recrystallized from EtOH. The deuterated analogues of DHA and TTBP were prepared following literature procedures.[17]

Physical Methods

Electronic absorption spectra were measured using a Hewlett-Packard 8453 diode array spectrophotometer equipped with liquid nitrogen cryostat (Unisoku) for temperature control. Resonance Raman spectra were recorded on an Acton AM-506 spectrophotometer, using a Kaiser Optical holographic supernotch filter with a Princeton Instruments LN/CCD-1100-PB/UVAR detector cooled with liquid nitrogen. Laser excitation was provided by a Spectra Physics 2060 Kr^+ laser. The spectra were obtained at 77 K and the Raman frequencies were referenced to indene. Electron paramagnetic resonance spectra were recorded on a Bruker EPP 300 spectrometer equipped with a liquid He cryostat.

Reactivity Studies

Tq samples for reactivity studies were prepared by first adding ~10 equiv of TBHP to 7 mM solutions of **1** in CH_2Cl_2 at −78 °C. The resulting solutions were placed overnight in a −80 °C freezer and then layer with cold pentane, resulting in precipitation of **Tq** after several days. After removal of solvent at −78 °C, the **Tq** solid was washed with pentane and then redissolved in cold PrCN. Small amounts (~0.1–0.2 mL) of this concentrated **Tq** solution were then directly transferred to UV-vis cuvettes (1 cm path length) cooled to −78 °C containing 2 mL of degassed PrCN, resulting in **Tq** concentrations of 0.3–0.7 mM. The resulting solutions were then subjected to several vacuum/backfill cycles with Ar to remove dissolved dioxygen. The cuvette was transferred to the low-temperature cryostat (set at either −70 or −45 °C) and substrate was added via syringe. Reaction progress was monitored with the UV-vis spectrometer described above.

The corresponding Fe^{IV}=O complexes (**3-X**) were generated in quartz cuvettes via two different procedures. The first involved addition of 4 equiv of TBHP to **1** in PrCN at −70 °C to give **2-PrCN**, followed by addition of excess pyridine to yield **3-pyr**. The second method involved addition of 4 equiv of TBHP to **1** in MeCN at −40 °C to give **2-MeCN**, followed by three-fold dilution with cold PrCN to yield **3-NCR.** After lowering the temperature to −70 °C, substrate was added via syringe and the reaction progress was monitored with UV-vis absorption spectroscopy.

Determination of reaction products and yields was carried out using gas chromatography, after first filtering solutions through silica gel to remove Fe salts. Naphthalene was employed as the internal standard.

Density Functional Theory Calculations

Geometry optimizations were performed with the Amsterdam Density Functional (ADF) 2006.01 software package[18] using ADF basis set IV (triple-ζ with single polarization), an integration constant of 4.0, and the Vosko-Wilk-Nusair local density approximation[19] with the nonlocal gradient corrections of Becke[20] and Perdew.[21] Cartesian coordinates for the DFT geometry-optimized models of **Tq** and **3-NCMe** are provided in Table S1(a–d).

Single-point DFT calculations (spin-unrestricted) were performed using the ORCA 2.4 software package developed by Dr. F. Neese.[22] The computations utilized Ahlrichs' valence triple-ζ basis set with one set of polarization functions (TZV/P) on all atoms, in conjunction with the corresponding auxiliary basis set (VTZ/C).[23] Extra polarization functions were included on the Fe and first-sphere ligand atoms. The calculations employed Becke's three-parameter hybrid functional for exchange[24,25] along with the Lee-Yang-Parr correlation functional[26] (B3LYP) with an integration grid of 4.0. The gOpenMol program developed by Laaksonen[27] was used to generate isosurface plots of molecular orbitals.

Results and Discussion

1. General Properties of Tq

As shown in Figure 1A, **Tq** exhibits two intense absorption features in the visible region at 645 and 840 nm (ε = 4.0 and 3.6 $mM^{-1}cm^{-1}$, respectively), which give the complex its bright turquoise color. Both bands likely arise from alkylperoxo→Fe^{IV} charge transfer transitions, as resonance Raman (rR) peaks corresponding to the ν(Fe-O) and ν(O-O) alkylperoxo modes are enhanced by excitation into these features.[10] Mössbauer studies of **Tq** confirmed the +4 oxidation state of the Fe center (δ = 0.10 mm/s; ΔE_Q = 1.76 mm/s) and revealed that the complex is low-spin (*S* = 1). For comparison, the corresponding Fe^{IV}=O complex (**3-MeCN**) is also low-spin with Mössbauer parameters δ = 0.07 mm/s and ΔE_Q = 1.02 mm/s.[10]

The redox potential of **Tq** was estimated with reductants of known oxidation potential. **Tq** is rapidly reduced by 1,1′-diacetylferrocene (490 mV vs. Fc/Fc^+) but fails to react with higher-potential reductants like tris(4-bromophenyl)amine (670 mV). Interestingly, **3-pyr** exhibits the same reactivity, suggesting that the redox potentials of both Fe^{IV} complexes lie between 490 and 670 mV.

2. Reaction of Tq with Phenols

The reactivity of **Tq** was first explored using the substrate 2,4,6-tri-*tert*-butylphenol (TTBP), which has proven a useful substrate for probing the H-atom abstracting ability of transition-metal complexes (the O-H bond dissociation energy, BDE, of TTBP is 81 kcal/mol[28]). While formation of **Tq** requires CH_2Cl_2 as solvent and a large excess of TBHP (Scheme 1), it is possible to isolate the complex by precipitation with pentane at −80 °C. The resulting solid can then be redissolved (without decomposition) into various other solvents, thereby yielding solutions of **Tq** with no excess oxidant. All samples employed in our reactivity studies were prepared in this manner, and the reactions were conducted under an inert atmosphere in butyronitrile (PrCN) at −70 °C – the highest temperature at which **Tq** is stable.

Figure 1A exhibits the changes observed in the UV-visible spectra upon addition of excess TTBP to **Tq**. The characteristic **Tq** absorption features at 840 and 645 nm decrease in intensity with concomitant formation of the phenoxyl radical peak at 402 nm. Based on the intensity of this feature (ε = 1.25 $mM^{-1}cm^{-1}$), the yield of the TTBP radical was determined to be 1.0 ± 0.1 equivalent, indicating that **Tq** functions as a one-electron oxidant. As evident in Figure 1B, both the decay of **Tq** and the formation of the phenoxyl radical follow pseudo first-order kinetics; variation of [TTBP] yielded a second-order rate constant of $3(1) \times 10^{-3}\ M^{-1}s^{-1}$ (Table

1; Figure S1A). Using d_1-TTBP as the substrate, a kinetic isotope effect (KIE) of ~2 was measured (Figure S1B), indicating that H-O bond cleavage is involved in the rate-limiting step. **Tq** reacts in a similar fashion with other substituted phenols, such as 2,6-di-*tert*-butylphenol (BDE = 83 kcal/mol) and 2,6-di-*tert*-butyl-4-methoxyphenol (BDE = 78 kcal/mol),[28] with reaction rates increasing with decreasing O-H BDE (Figure S2).[29]

While a concerted H-atom transfer mechanism is supported by the strong dependence of rates on H-O BDE and the observed KIE for TTBP oxidation, two alternatives were also considered. The first involves fast electron transfer followed by rate-limiting proton transfer; however, this possibility seems unlikely given that **Tq** fails to oxidize tris(4-bromophenyl)amine, which has a much lower potential (0.67 V) than the substrates (1.0 V for TTBP,[30] ~1.4 V for DHA[31]). The second alternative mechanism involves rate-limiting proton transfer followed by fast electron-transfer. Yet this mechanism is disfavored by the low basicity of **Tq**, as evidenced by the fact the addition of excess HBF^4 at −70 °C results in no spectral changes.

The isosbestic point at 590 nm (Figure 1A) indicates that TTBP cleanly reduces **Tq** to the product complex, which exhibits a single intense visible band at 600 nm (ε = 2.5 $mM^{-1}cm^{-1}$). Significantly, the absorption spectrum of the product is identical to the one reported, in our previous study, for $[Fe^{III}(\beta\text{-BPMCN})(OO^tBu)(PrCN)]^{2+}$ (**2-PrCN**).[10] EPR and rR spectra obtained with the product solutions (Figures S3 and S4, respectively) provide further evidence that **2-PrCN** is the sole Fe-containing product of the reaction of **Tq** with phenols. Thus, the alkylperoxo ligand remains intact and coordinated to the Fe center during the course of the reaction. We therefore conclude that abstraction of the phenolic H is carried out by the Fe^{IV}-OH unit of **Tq** to yield the complex $[(L)Fe^{III}(OO^tBu)(OH_2)]^{2+}$, which in PrCN undergoes rapid ligand substitution to give **2-PrCN** (Scheme 2).

3. Reaction of Tq Intermediate with Hydrocarbons

At −70 °C, **Tq** exhibits only sluggish reactivity towards hydrocarbons with weak C-H bonds, such as 9,10-dihydroanthracene (DHA; BDE = 78 kcal/mol) and 1,4-cyclohexadiene (1,4-CHD; BDE = 77 kcal/mol).[32] Both substrates reduce **Tq** to the corresponding alkylperoxoiron (III) complex **2-PrCN**, as was found to be the case with phenols (*vide supra)*. In the case of DHA, the reaction yields 0.53 ± 0.08 equivalents of anthracene per **Tq** as determined by the intensity of the absorption feature at 378 nm (Figure 2), providing further evidence that **Tq** behaves as a one-electron oxidant. When the reaction with DHA is performed in CH_2Cl_2, a non-coordinating solvent, the absorption feature of the product complex is blue-shifted to 530 nm (Figure S5). This chromophore corresponds to the high-spin complex **2-OH_2**',[10] thus proving that H-atom transfer initially generates an Fe^{III}-OH_2 complex (Scheme 2).

A detailed kinetic analysis of the **Tq** + DHA reaction was hindered by the exceptionally slow nature of the reaction rate, combined with the low solubility of DHA in PrCN at −70 °C. Nevertheless, using the method of initial rates, it was possible to estimate a rate constant of $k_2 = (1.5 \pm 0.5) \times 10^{-3}\ M^{-1}s^{-1}$ (Table 1). With d_4-DHA as substrate, a KIE value of approximately 3 was measured (Figure 3), indicating that C-H bond activation is the rate-limiting step. For both DHA and 1,4-CHD, the reaction with **Tq** is first-order with respect to substrate concentration. Interestingly, **Tq** is more reactive towards DHA than 1,4-CHD, despite the fact that the two substrates possess nearly identical C-H BDE's.

At −70 °C, **Tq** is unreactive towards hydrocarbons with C-H BDE's greater than 80 kcal/mol, such as cyclohexene and toluene. In contrast, it has been shown that these substrates are readily oxidized by various Fe^{IV}=O complexes, albeit at higher temperatures.[12] Thus, the Fe^{IV}-OH moiety of **Tq** appears to exhibit diminished reactivity relative to Fe^{IV}=O units – a result that is confirmed in the following section.

4. Comparison with $[Fe^{IV}(\beta\text{-BPMCN})(O)]^{2+}$ (3) Reactivity

As shown in Scheme 1, treatment of $Fe^{II}(\beta\text{-BPMCN})(OTf)_2$ (**1**) with TBHP at −40 °C in MeCN generates the corresponding alkylperoxoiron(III) complex, which slowly converts to the oxoiron(IV) complex **3-MeCN** via O-O bond homolysis. To directly compare its reactivity with **Tq** at −70 °C, though, it was necessary to prepare **3** in PrCN. This was accomplished with two different methods. The first involved direct addition of TBHP to solutions of **1** in PrCN. However, it was found that smooth conversion of **2-NCPr** to **3** required addition of pyridine, presumably to yield **3-pyr**. This "push effect" of Lewis bases was observed previously in the homolysis of Fe^{III}-OOR intermediates generated with TPA – another tetradentate supporting ligand that permits *cis*-coordination of exogenous ligands.[33] The second method involved first generating **3** in MeCN and then diluting the solution with excess PrCN to give **3-NCR**.

Both oxoiron(IV) complexes (**3-pyr** and **3-NCR**) react rapidly with TTBP even at −70 °C, as determined by decay of the NIR feature at 750 nm and concomitant formation of the TTBP radical signal (Figure S6). The reaction is first-order with respect to **3** and TTBP, although accurate assessment of rates was complicated by the rapid nature of the reaction, which may introduce errors due to mixing times. Despite this, an overall second-order rate constant of ~15 $M^{-1}s^{-1}$ was determined, indicating that the Fe^{IV}=O unit of **3** is more than 10^3 times more reactive towards TTBP than the Fe^{IV}-OH unit of **Tq** (Table 1). Slightly higher rates were measured for **3- NCR** than **3-pyr**, indicating that the reaction does not operate through a base-assisted pathway (**3-pyr** is prepared in the presence of a large excess of pyridine). Further support for a direct H-atom transfer mechanism comes from the KIE value of 4 measured for **3-NCR** with TTBP (Table 1; Figure S7).

The much greater H-atom abstracting ability of **3** relative to **Tq** was also observed for hydrocarbon substrates. The second-order rate constant for the reaction of **3-pyr** with DHA was found to be 0.14(1) $M^{-1}s^{-1}$ – a nearly 100-fold increase over the **Tq** value (Table 1). This reaction also exhibits a large nonclassical KIE of 200 (Figure 3), which is a common feature of Fe^{IV}=O reactivity towards C-H bonds.[12,13,15] For 1,4-CHD, the disparity in oxo-versus-hydroxo rates is even greater than for DHA, with a k(**3**)/k(**Tq**) value of 200 (Table 1). Moreover, unlike **Tq**, **3-pyr** is capable of oxidizing substrates with C-H bonds > 80 kcal/mol. For instance, **3-pyr** reacts with cyclohexene (BDE = 87 kcal/mol) at −70 °C ($k_2 = 2 \times 10^{-4}$ $M^{-1}s^{-1}$) to yield the allylic oxidation products 2-cyclohexen-1-ol and 2-cyclohexen-1-one.

Our results are generally consistent with kinetic data published by Busch and coworkers for the series of Mn^{IV} complexes $[(EBC)Mn^{IV}(OH)_2]^{2+}$, $[(EBC)Mn^{IV}(O)(OH)]^{+}$, and $(EBC)Mn^{IV}(O)_2$ (where EBC is the cross-bridged cyclam ligand 4,11-dimethyl-1,4,8,11-tetraazabicyclo- [6.6.2]hexadecane). Using various substrates, it was found that the mono- and dioxo Mn^{IV} complexes perform H-atom abstractions approximately 15 and 40 times faster, respectively, than the corresponding dihydroxo complex (Table 1).[8,9] Interestingly, our findings indicate that the disparity in oxo/hydroxo rates is even larger in Fe^{IV} systems. Furthermore, the reactivity of **Tq** towards hydrocarbons *at −70 °C* is roughly the same as the reactivity of $[Mn^{IV}(OH)_2]^{2+}$ *at room temperature*, pointing to greater intrinsic oxidizing power of Fe^{IV} relative to Mn^{IV}.

5. Reactivity of Tq at Elevated Temperatures

As noted above, **Tq** exhibits no reactivity at −70 °C towards hydrocarbons with C-H BDE's > 80 kcal/mol. To determine whether this lack of reactivity was merely due to the low temperatures employed, experiments were carried out at −45 °C in PrCN under an Ar atmosphere. At this higher temperature, **Tq** self-decays at a rate of $1.3(2) \times 10^{-3}$ s^{-1}. However, the reaction does not yield the alkylperoxoiron(III) complex **2-PrCN**; instead, the absorption

spectrum of the final solution is nearly featureless (Figure S8), indicating loss of the alkylperoxo-to-iron charge transfer transitions.

At −45 °C **Tq** decay in the presence of hydrocarbons with BDE's > 80 kcal/mol results in their oxidation (Table 2). For example, for cyclohexene (BDE = 87 kcal/mol), the reaction carried out under Ar yielded 1.0(2) equiv 2-cyclohexen-1-ol and 0.4(1) equiv 2-cyclohexen-1- one per **Tq** (and no epoxide). The same reaction performed in air afforded ketone as the dominant product and nearly 5 equiv cyclohexene oxidized per **Tq** (Table 2). The dramatic increase in the ketone yield in air and the corresponding change in the alcohol/ketone ratio indicate that long-lived cyclohexenyl radicals are formed initially. More importantly, it is clear that more than 1 equiv cyclohexenyl radical is produced under Ar, suggesting that **Tq** decomposition creates more than one equivalent of oxidant capable of H-atom abstraction from cyclohexene. **Tq** decomposition also generates species capable of oxo transfer to styrene and *cis*-stilbene yielding the corresponding epoxides (Table 2). The epoxide yields were lower than the allylic oxidation yields for cyclohexene, and some loss of stereochemistry was observed in the case of *cis*-stilbene. The fact that cyclohexene oxide is not formed at all in the course of cyclohexene oxidation suggests that the oxidants formed during **Tq** decay appear to favor H-atom abstraction over oxo transfer.

Kinetic studies in the presence of substrates show that **Tq** decay is independent of both substrate identity and concentration. Thus, ***Tq*** *itself is not the active species in hydrocarbon oxidation*. Instead, **Tq** must first convert – in the rate-limiting step – to more reactive species that can carry out H-atom abstraction and olefin epoxidation. The nature of the active oxidant(s) is currently unknown. We demonstrated above that at −70 °C the Fe-OO^{t}Bu unit is stable and unreactive. However, this unit decomposes at − 45 °C with loss of the alkylperoxo-to-iron charge transfer band, so it is likely that the Fe^{IV}-OOR unit fragments upon warming. Fragmentation of the alkylperoxoiron(IV) unit can proceed along three possible pathways, as shown in Scheme 3: (i) homolytic O-O cleavage to yield *tert*-butoxyl radical and an Fe^{V}(O)(OH) species, (ii) heterolytic O-O cleavage to give an Fe^{VI}(O)(OH) species, or (iii) Fe-OOR cleavage to provide an alkylperoxyl radical. Previous studies of transition-metal/TBHP systems have demonstrated that alkoxyl and alkylperoxyl radicals are often the active species in hydrocarbon oxidation and responsible for the generation of long-lived alkyl radicals.[34–36] Such chemistry is consistent with that observed for cyclohexene oxidation by the **Tq** system at −45 °C, yet the formation of *cis*-stilbene oxide from *cis*-stilbene (Table 2) requires formation of an Fe=O species capable of direct O-atom transfer to substrate with retention of configuration. We thus favor option (i) above as the dominant decomposition mechanism for **Tq** at −45 °C that accounts for all the experimental observations. This mechanism would produce two oxidants, both of which can act as H-atom abstraction agents, and thus rationalize the formation of more than one equivalent of oxidized product from cyclohexene.

6. Electronic Structure Analysis

The electronic structures the (S = 1) Fe^{IV} complexes **Tq** and **3** were analyzed with density functional theory (DFT) with the aim of gaining insight into their contrasting reactivities. As the BPMCN ligand is the *cis*-β conformation, the two labile coordination sites are distinct and two positional isomers exist for each complex. For **Tq** (and **3**), the isomers have been labeled A and B depending on whether the hydroxo (or oxo) ligand is *trans* to the pyridyl (A) or the amino (B) moiety (see Scheme 4). Full geometry optimizations were performed for both **Tq** isomers, although the cyclohexane ring was replaced with a simple –CH_2CH_2– bridge. The resulting Fe-ligand bond distances, as well as the orientations of the ^{t}BuOO group, are nearly identical for both isomers. While isomer B is slightly more stable (0.7 kcal/mol), the difference is well within the error of DFT, further supporting the earlier conclusion (derived from spectroscopic data) that **Tq** solutions contain roughly equal amounts of both isomers.[10] In the

optimized structures (**Tq^{A}** and **Tq^{B}**), the two Fe-O bond distances are approximately 1.8 Å and the four Fe-N bond distances were found to be 2.05 ± 0.07 Å, in excellent agreement with the EXAFS data (2 N/O scatterers at 1.82 Å, 3 N/O scatterers at 2.01 Å). The short Fe^{IV}-O_p bond distance of ~1.82 Å (O_p = proximal O of alkylperoxo ligand) and O-O distance of ~1.42 Å are similar to values calculated for low-spin Fe^{III}-alkylperoxo complexes.[37] The calculations also suggest that the hydroxo ligand is capable of forming a weak hydrogen-bond with the distal oxygen (O_d) of the alkylperoxo ligand, which may control the relative orientation of the O^{t}Bu group.

Geometry optimizations were also carried out for the Fe^{IV}=O complex **3-NCMe**. As with **Tq**, the resulting structural parameters and molecular energies were virtually identical for the two isomers (**3^{A}-NCMe** and **3^{B}-NCMe**). The computed Fe=O and Fe-N bond distances of 1.65 and ~2.06 Å, respectively, are consistent with the **3-NCMe** EXAFS data as well as previously reported experimental and computational structures of Fe^{IV}=O complexes.[11,38,39]

Figure 4 depicts the relevant portion of molecular orbital (MO) energy level diagram for model **Tq^{B}**. The most appropriate molecular orientation places the z-axis along the N_{pyr}-Fe- N_{amine} bonds, while the hydroxo and alkylperoxo ligands lie in the xy-plane (Scheme 4). As **Tq** is a low-spin (S = 1) complex, the Fe(xy)-based MO is doubly-occupied, while the high-energy Fe(x^2-y^2)- and Fe(z^2)-based MOs are unoccupied. The two *unpaired* electrons lie in orbitals with Fe(xz/yz) character that participate in π-interactions with either the alkylperoxo (113-β) or hydroxo (114-β) ligands (Figure 4). The π-interaction between the Fe(xz) and peroxo(π_v^*) orbitals is particularly strong and covalent, with MO 113-β containing 39% Fe and 53% OO^{t}Bu character (a similarly covalent Fe/O π-interaction is characteristic of low-spin *ferric*-alkylperoxo systems[37]). By comparison, the Fe-OH bond in **Tq** is more ionic, with MO 114-β containing 73% Fe and only 20% OH character.

H-atom abstraction reactions proceed via donation of electron density from the substrate H-X bond into a low-lying unoccupied orbital on the oxidant. For this reason, it is possible to rationalize the H-atom abstracting ability of transition-metal complexes by analysis of their frontier molecular orbitals (FMOs), particularly those lowest-energy unoccupied MOs (LUMOs) that can serve as acceptor orbitals. Indeed, a recent study of transition-metal oxo species by Michel *et al.* demonstrated that the activation barrier for H-atom abstraction is directly controlled by the energy and shape of the acceptor orbital(s).[40] More specifically, Solomon and coworkers have shown that the reactivity of low-spin Fe^{IV}=O complexes towards C-H bonds is proportional to the amount of oxo character in the spin-down (β) Fe/O(π*) orbitals, which are the LUMOs.[41,42] The oxo character is important because *FMO theory requires the acceptor orbital to have significant electron density on the reactive atom* in order to maximize overlap between the donor and acceptor orbitals.

For the **Tq** models, the LUMO is the π* orbital (113-β) localized on the Fe-O-O unit. Thus, it might be expected that **Tq** would react with H-X bonds to yield the Fe^{III} complex, HOO^{t}Bu, and the substrate radical. However, it appears that 113-β is not a viable acceptor orbital for steric reasons. Access to the proximal O-atom, which contains the largest lobe of electron density (35% of MO β-113), is blocked by both the *tert*-butyl group and substituents on the BPMCN ligand (a pyridyl ring for **Tq^{A}** and a methyl group for **Tq^{B}**). And while the Fe^{III}-OOH intermediate of activated bleomycin has been postulated to directly abstract a H-atom from DNA[7,42] the acceptor orbital in that system is the O-O σ* orbital, not the π* orbital. For **Tq**, the O-O σ* orbital is high in energy (4.7 eV above the LUMO) and its access to substrate is also blocked by the ^{t}Bu group.

The second lowest unoccupied MO for **Tq** is the π* orbital of the Fe-OH bond (114- β), which lies 0.7 eV higher in energy than 113-β. The hydroxide ligand is well-exposed to solvent, but

this accessibility is partially offset by the small amount of OH character in the MO (20%). Thus, the elevated energy of the acceptor MO and the low MO coefficients on the hydroxide ligand combine to limit the oxidizing power of the Fe^{IV}-OH unit.

Like all low-spin Fe^{IV}=O complexes studied to date, **3^{B}-NCMe** possesses a $(xy)^2(xz)^1(yz)^1$ configuration in which Fe(xz/yz) orbitals participate in highly covalent π-interactions with the O(p_x/p_y) orbitals (Figure 5). Indeed, our calculations indicate that the two spin-down Fe/O (π*) orbitals (99-β and 100-β), which are nearly isoenergetic, contain approximately 50% Fe and 40% O character. These orbitals are the LUMOs and thus serve as the acceptor orbitals in H-atom abstraction reactions. As noted above, the large degree of oxo character in these orbitals facilitates the H-atom abstraction and accounts for the remarkable oxidizing ability of **3^{B}-NCMe**. The contrast between the electronic structures of **Tq^{B}** and **3^{B}-NCMe** is especially evident in Figure 6, which displays contour plots of the total unpaired spin density for both complexes (note that since the putative acceptor orbitals are the singly-occupied MOs in both cases, plots of spin density correspond to the spatial distribution of the FMOs). **3^{B}-NCMe** has a large lobe of unpaired spin density (43% of the total) that is localized on the oxo ligand and easily accessible to substrates – the ideal scenario for facile H-atom abstraction. By contrast, the unpaired spin density in **Tq** is much more diffuse, with no ligand atom carrying more than 18% of the total; indeed, only 10% is localized on the reactive hydroxo ligand. Collectively, these results indicate that protonation of the ferryl unit substantially decreases the covalency of the Fe/O bond, thereby diminishing the amount of oxygen character in the LUMOs. As these orbitals serve as the acceptor orbitals for H-atom abstraction, this dramatic change in Fe-O bonding explains the massive disparities in reactivity reported above.

While FMO theory accounts for the increased *kinetic* reactivity of **3** relative to **Tq**, it does not address the related *thermodynamic* issue; i.e., the fact that **Tq** cannot oxidize C-H bonds stronger than ~80 kcal/mol whereas **3-pyr** oxidizes the stronger C-H bonds of cyclohexene at −70 °C. This matter is determined by the dissociation energy of the H-O bonds of the resulting Fe^{III} species. For the complexes discussed here, the strength of the H-O bond formed during H-atom abstraction is proportional to (i) the one-electron redox potential of the Fe^{IV} oxidant, and (ii) the pK_a of the Fe^{III}-$OH_{(1\ or\ 2)}$ product complex. The exact formula is provided below:[43–45]

$$D(O-H)=23.06\times E^{o}(Fe^{IV}/Fe^{III}\ vs.\ Fc^{+}/Fc)+1.37\,pK_a(Fe^{III}-OH_{(1\ or\ 2)})+59.5\ kcal/mol \quad (5)$$

While precise E^0 values for **Tq** and **3** are not known, our results indicate that both potentials fall within the range of 490–670 mV, suggesting that the observed differences in H-atom abstracting power are not determined by redox potential. Instead, the second term in eq. 5 likely plays the decisive role, as the [Fe^{III}-OH_2] unit formed by **Tq + H•** is undoubtedly much more acidic than the [Fe^{III}-OH] unit formed by **3 + H•**. Thus, the basicity of the one-electron reduced Fe^{III}-O^{-} complex provides much of the driving force for the remarkable H-atom abstracting ability of **3**. The importance of oxo ligand basicity in H-atom abstraction reactions has been highlighted by others in recent studies of Mn-oxo reactivity.[9,46,47]

Summary

Tq is a novel Fe^{IV} complex with both alkylperoxo and hydroxo ligands. Here, we showed that **Tq** reacts at −70 °C with substrates with weak H-X bonds (like TTBP and DHA) to yield the corresponding alkylperoxoiron(III) complex **2-PrCN**, indicating that an H-atom from substrate is transferred to the Fe^{IV}-OH unit (Scheme 2). We then compared the reactivity of **Tq** with that of complex **3**, which features an Fe^{IV}=O moiety supported by the same ligand. Even with

a limited number of substrates, our kinetic studies clearly demonstrate that **3** is far more reactive than **Tq** towards H-atom donors, by as much as a factor of 10^3 (Table 1). The differing H-atom abstracting abilities of **3** and **Tq** are related to their underlying electronic structures, as elucidated with DFT methods. Due to the highly covalent nature of the Fe^{IV}=O π-bonds, **3** features two low-lying acceptor MOs with substantial oxo-character, thereby facilitating the electrophilic attack of H-X bonds. However, protonation of the ferryl to give an Fe^{IV}-OH unit disrupts this felicitous situation in two respects: (i) the hydroxo ligand can have only one π-interaction with the Fe center (versus two for the oxo ligand), and (ii) the proton lowers the energy of the remaining O(p) orbital, resulting in diminished Fe-O covalency and less OH character in the acceptor MO. Hence, we have the (counterintuitive) result that protonation of the ferryl unit makes it *less* electrophilic towards H-atom donors. This trend is also observed by Busch and co-workers in their study of Mn^{IV}(EBC) complexes.[9]

In contrast to the remarkable oxidizing power of **3** and other Fe^{IV}=O complexes, **Tq** is only capable of oxidizing hydrocarbons with weak C-H bonds (< 80 kcal/mol). However, at elevated temperatures, **Tq** decays to form one or more reactive species that oxidize more demanding substrates (Table 2). Based on spectroscopic and reactivity data, we conclude that the active species is generated by fragmentation of the alkylperoxoiron(IV) unit (Scheme 3). Indeed, this scenario is consistent with previous studies where Fe^{III}- and Cu^{II}-alkylperoxo complexes were found to be inert but gave rise to very reactive intermediates via O-O bond homolysis.[48–50]

The results presented here have several implications for metalloenzyme systems involved in H-atom abstraction. First, and most important, is the conclusion that Fe^{IV}-OH intermediates are significantly less reactive than Fe^{IV}=O intermediates. Thus, it is not surprising that only one class of enzymes – the lipoxygenases – is known to employ an Fe-OH species as the reactive intermediate for H-atom abstraction. And, in this case, the target C-H bond of the fatty acid substrate is quite weak (estimated BDE ~76 kcal/mol) due to its bis-allylic position.[6] Interestingly, despite its higher oxidation state, the reactivity of **Tq** is comparable to that of the lipoxygenase model complex [(PY5)Fe^{III}-OH] (PY5 = 2,6-bis(bis(2-pyridyl)methoxy-methane) pyridine), which is also limited to oxidizing weak C-H bonds.[51] While the oxidation potential of **Tq** is at least 0.25 V more positive than the value measured for [(PY5)Fe^{III}-OH], this factor is likely offset by the increased basicity of the hydroxo ligand in the more reduced complex. Thus, it appears that Fe-OH species exhibit sluggish H-atom abstraction reactivity regardless of oxidation state.

Secondly, our study of the Fe^{IV}-OH unit of **Tq** has implications for diiron enzymes, such as MMO and RNR, in which the putative reactive oxo ligand is located in a bridging position between the two Fe centers. This comparison is valid because the second Fe center can be thought of as a weakly-bound proton (i.e., Fe^{IV}–O–H ≈ Fe^{IV}–O–Fe). Inspection of DFT results published by Solomon and coworkers for the hypothetical complex [$Fe^{III}Fe^{IV}$(μ-O)(μ-$OAc)_2(L)_2]^{3+}$ (L = 9-crown-3-ether), suggests that Fe^{III} centers perturb the Fe^{IV}-oxo unit in a manner similar to that described here for protons.[52] For instance, relative to the mononuclear Fe^{IV}=O system, coordination of the second Fe center lengthens the Fe^{IV}-O bond and diminishes the amount of O(p) character in the LUMOs. However, it is also clear that metal binding does not disrupt the oxoiron(IV) unit to the same extent as proton binding.[53] Whereas the additional Fe center merely perturbs the π-interactions of the oxoiron(IV) unit, the O→OH conversion fundamentally destroys the covalent nature of the Fe^{IV}=O bond. Thus, based on our analysis, we predict that bridging oxo ligands are generally *more reactive* than terminal hydroxo ligands but *less reactive* than terminal oxo ligands. Support for this conclusion comes from our recent study of a synthetic model that, like intermediate **Q,** possesses a [$Fe^{IV}{}_2$(μ-$O)_2$] diamond core. This complex was found to be 80-fold less reactive toward DHA than the corresponding mononuclear Fe^{IV}=O complex.[54] This finding, combined with the results presented here

regarding an Fe^{IV}-OH species, suggests the following order of reactivity for Fe^{IV} intermediates:

$$Fe^{IV}=O \gg Fe^{IV}-O-Fe > Fe^{IV}-OH$$

We therefore conclude that the coordination of Lewis acids, whether protons or metals ions, to oxoiron(IV) units dramatically reduces their oxidizing power.

Supplementary Material

Refer to Web version on PubMed Central for supplementary material.

Acknowledgments

This research was supported by the National Institutes of Health (grant GM-33162 to L.Q. and postdoctoral fellowship GM-079839 to A.T.F.). We thank Professor Thomas Brunold of the University of Wisconsin-Madison for graciously providing access to his computer cluster.

References

1. Costas M, Mehn MP, Jensen MP, Que L Jr. Chem Rev 2004;104:939–986. [PubMed: 14871146]
2. Groves JT. J Inorg Biochem 2006;100:434–447. [PubMed: 16516297]
3. Sono M, Roach MP, Coulter ED, Dawson JH. Chem Rev 1996;96:2841–2887. [PubMed: 11848843]
4. Krebs C, Galonić Fujimori D, Walsh CT, Bollinger JM Jr. Acc Chem Res 2007;40:484–492. [PubMed: 17542550]
5. Tshuva EY, Lippard SJ. Chem Rev 2004;104:987–1012. [PubMed: 14871147]
6. Nelson, MJ.; Seitz, SP. Active Oxygen in Biochemistry. Valentine, JS.; Foote, CS.; Greenberg, A.; Liebman, JF., editors. Chapman & Hall; London: 1995. p. 276-312.
7. Decker A, Chow MS, Kemsley JN, Lehnert N, Solomon EI. J Am Chem Soc 2006;128:4719–4733. [PubMed: 16594709]
8. Yin G, Danby AM, Kitko D, Carter JD, Scheper WM, Busch DH. J Am Chem Soc 2007;129:1512–1513. [PubMed: 17249671]
9. Yin GC, Danby AM, Kitko D, Carter JD, Scheper WM, Busch DH. J Am Chem Soc 2008;130:16245–16253. [PubMed: 18998682]
10. Jensen MP, Costas M, Ho RYN, Kaizer J, Mairata i Payeras A, Münck E, Que L Jr, Rohde J-U, Stubna A. J Am Chem Soc 2005;127:10512–10525. [PubMed: 16045338]
11. Jackson TA, Rohde JU, Seo MS, Sastri CV, DeHont R, Stubna A, Ohta T, Kitagawa T, Munck E, Nam W, Que L. J Am Chem Soc 2008;130:12394–12407. [PubMed: 18712873]
12. Kaizer J, Klinker EJ, Oh NY, Rohde JU, Song WJ, Stubna A, Kim J, Münck E, Nam W, Que L Jr. J Am Chem Soc 2004;126:472–473. [PubMed: 14719937]
13. Oh NY, Suh Y, Park MJ, Seo MS, Kim J, Nam W. Angew Chem Int Ed 2005;44:4235–4239.
14. Sastri CV, Lee J, Oh K, Lee YJ, Lee J, Jackson TA, Ray K, Hirao H, Shin W, Halfen JA, Kim J, Que L Jr, Shaik S, Nam W. Proc Natl Acad Sci USA 2007;104:19181–19186. [PubMed: 18048327]
15. Klinker EJ, Shaik S, Hirao H, Que L. Angew Chem Int Ed 2009;48:1291–1295.
16. Costas M, Rohde JU, Stubna A, Ho RYN, Quaroni L, Münck E, Que L Jr. J Am Chem Soc 2001;123:12931–12932. [PubMed: 11749564]
17. Goldsmith CR, Jonas RT, Stack TDP. J Am Chem Soc 2002;124:83–96. [PubMed: 11772065]
18. ADF2006.01; SCM, Theoretical Chemistry. Vrije Universiteit; Amsterdam, The Netherlands: http://www.scm.com
19. Vosko SH, Wilk L, Nusair M. Can J Phys 1980;58:1200.
20. Becke AD. J Chem Phys 1986;84:4524–4529.
21. Perdew JP. Phys Rev B 1986;33:8822–8824.

22. Neese, F. version 2.5 ed. University of Bonn; Bonn, Germany: 2006.
23. Schafer A, Horn H, Ahlrichs R. J Chem Phys 1992;97:2571–2577.
24. Becke AD. J Chem Phys 1993;98:5648–5652.
25. Becke AD. J Chem Phys 1993;98:1372–1377.
26. Lee CT, Yang WT, Parr RG. Phys Rev B 1988;37:785–789.
27. Laaksonen L. J Mol Graph 1992;10:33. [PubMed: 1504051]
28. Lucarini M, Pedrielli P, Pedulli GF, Cabiddu S, Fattuoni C. J Org Chem 1996;61:9259–9263.
29. Pseudo first-order rate constants for these 2,6-di-*tert*-butyl-4-X-phenols were measured at similar substrate concentrations. For X = H, $k_1 = 0.99 \times 10^{-4}$ s^{-1} at 50 mM; for X = tBu, $k_1 = 2.7 \times 10^{-4}$ s^{-1} at 59 mM; for X = OMe, $k_1 = 27 \times 10^{-4}$ s^{-1} at 39 mM.
30. Bordwell FG, Cheng JP. J Am Chem Soc 1991;113:1736–1743.
31. Schlesener CJ, Amatore C, Kochi JK. J Am Chem Soc 1984;106:3567–3577.
32. Laarhoven LJJ, Mulder P, Wayner DDM. Acc Chem Res 1999;32:342–349.
33. Kaizer J, Costas M, Que L Jr. Angew Chem Int Ed 2003;42:3671–3673.
34. MacFaul PA, Arends IWCE, Ingold KI, Wayner DDM. J Chem Soc, Perkin Trans 1997;2:135–145.
35. MacFaul PA, Ingold KU, Wayner DDM, Que L Jr. J Am Chem Soc 1997;119:10594–10598.
36. Caudle MT, Riggs-Gelasco P, Gelasco AK, Penner-Hahn JE, Pecoraro VL. Inorg Chem 1996;35:3577–3584.
37. Lehnert N, Ho RYN, Que L Jr, Solomon EI. J Am Chem Soc 2001;123:8271–8290. [PubMed: 11516278]
38. Rohde JU, In JH, Lim MH, Brennessel WW, Bukowski MR, Stubna A, Münck E, Nam W, Que L Jr. Science 2003;299:1037–1039. [PubMed: 12586936]
39. Klinker EJ, Kaizer J, Brennessel WW, Woodrum NL, Cramer CJ, Que L Jr. Angew Chem Int Ed 2005;44:3690–3694.
40. Michel C, Baerends EJ. Inorg Chem 2009;48:3628–3638. [PubMed: 19301854]
41. Decker A, Rohde J-U, Klinker EJ, Wong SD, Que L Jr, Solomon EI. J Am Chem Soc 2007;129:15983–15996. [PubMed: 18052249]
42. Solomon EI, Wong SD, Liu LV, Decker A, Chow MS. Curr Opin Chem Biol 2009;13:99–113. [PubMed: 19278895]
43. Bordwell FG, Cheng JP, Ji GZ, Satish AV, Zhang X. J Am Chem Soc 1991;113:9790–9795.
44. Parker VD Jr, Handoo KL, Roness F, Tilset M. J Am Chem Soc 1991;113:7493–7498.
45. Gardner KA, Mayer JM. Science 1995;269:1849–1851. [PubMed: 7569922]
46. Parsell TH, Yang MY, Borovik AS. J Am Chem Soc 2009;131:2762–2763. [PubMed: 19196005]
47. Lansky DE, Goldberg DP. Inorg Chem 2006;45:5119–5125. [PubMed: 16780334]
48. Seo MS, Kamachi T, Kouno T, Murata K, JPM, Yoshizawa K, Nam W. Angew Chem Int Ed 2007;46:2291–2294.
49. Kunishita A, Ishimaru H, Nakashima S, Ogura T, Itoh S. J Am Chem Soc 2008;130:4244–4245. [PubMed: 18335943]
50. Kitajima N, Katayama T, Fujisawa K, Iwata Y, Morooka Y. J Am Chem Soc 1993;115:7872–7873.
51. Goldsmith CR, Stack TDP. Inorg Chem 2006;45:6048–6055. [PubMed: 16842013]
52. Decker A, Clay MD, Solomon EI. J Inorg Biochem 2006;100:697–706. [PubMed: 16510189]
53. In the [Fe^{III}-O-Fe^{IV}] complex, the O(p) orbital directed towards the second Fe center still participates in π-bonding with the Fe^{IV} center, whereas the corresponding orbital in the Fe^{IV}-OH unit interacts too strongly with the H to allow for significant bonding to the Fe center.
54. Xue G, Wang D, De Hont R, Fiedler AT, Shan X, Münck E, Que L Jr. Proc Natl Acad Sci USA 2007;104:20713–20718. [PubMed: 18093922]

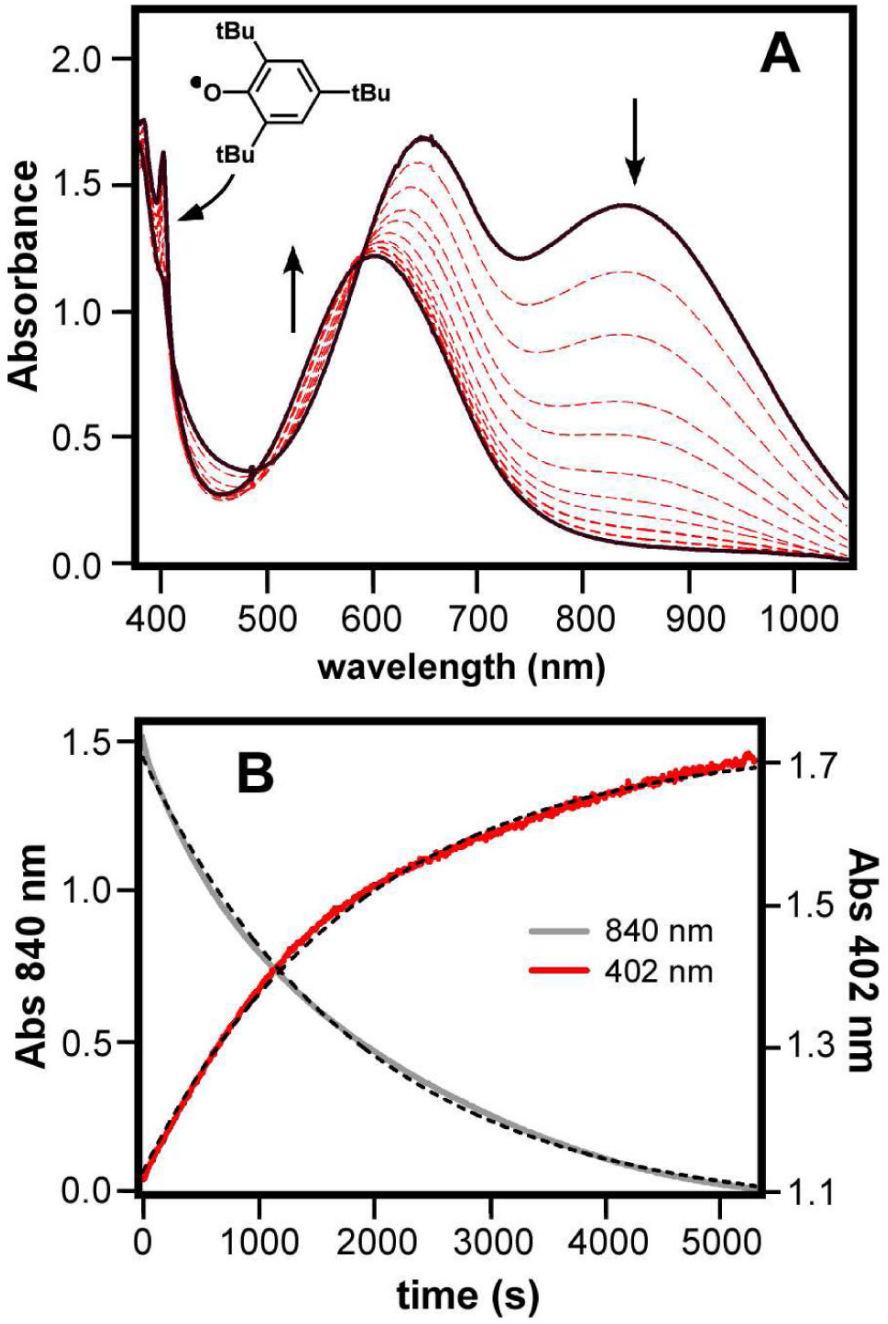

Figure 1.

(A) UV-vis absorption spectra of the reaction of **Tq** with TTBP at −70 °C in PrCN ([TTBP] = 150 mM, $[\mathbf{Tq}]_0$ = 0.43 mM). (B) Plot of absorption intensities at 840 nm (solid black) and 402 nm (solid red) as a function of time for the reaction shown above. The dashed lines represent first-order kinetic fits ($k_1 = 5.3 \times 10^{-4}$ s^{-1} for both traces).

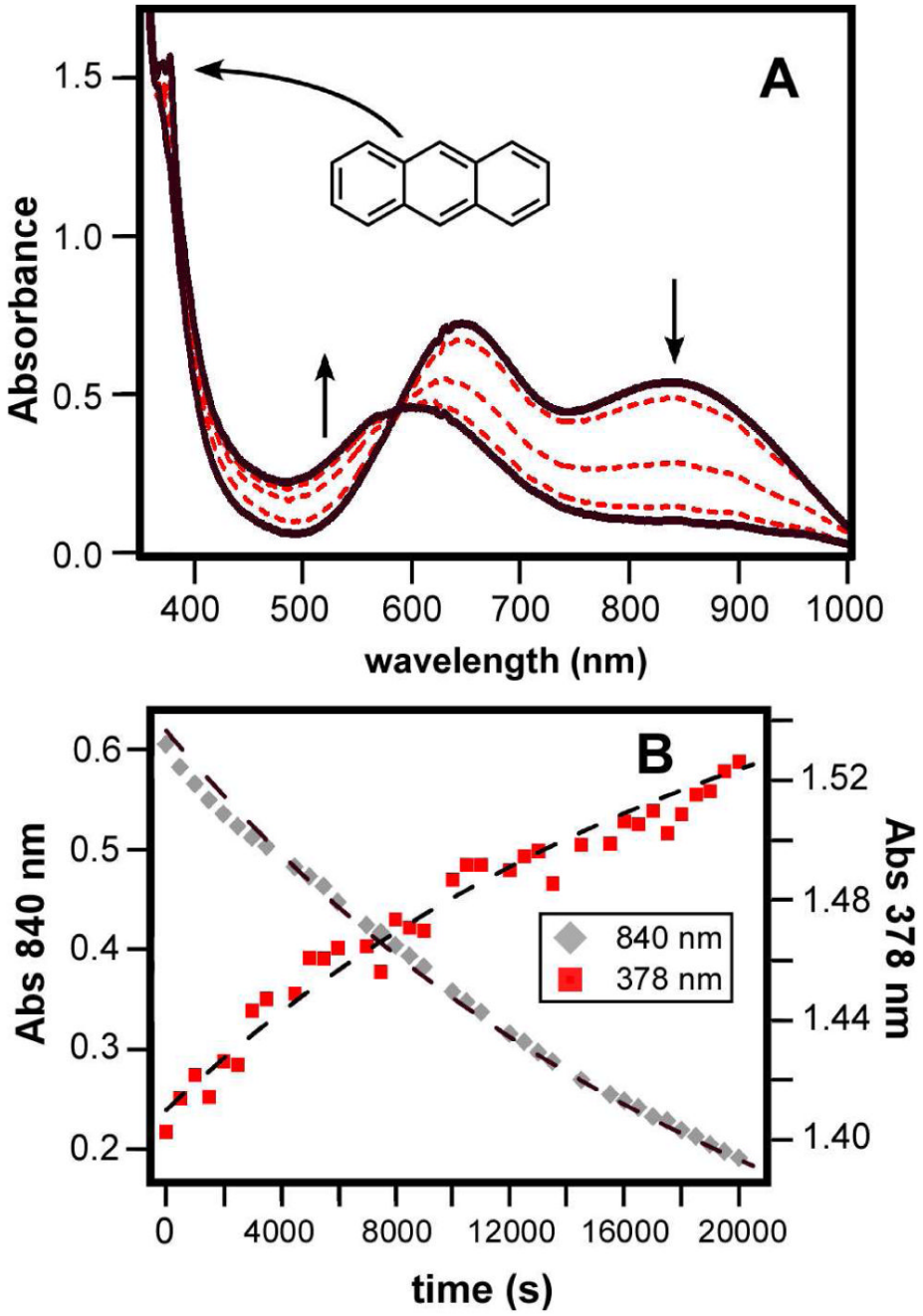

Figure 2.

(A) UV-vis absorption spectra of the reaction of **Tq** with DHA at −70 °C in PrCN ([DHA] = 24 mM, $[\mathbf{Tq}]_0$ = 0.15 mM). (B) Plot of absorption intensities at 840 nm (solid black) and 378 nm (solid red) as a function of time for the reaction shown above; both traces were adjusted to remove changes in baseline intensity. The dashed lines represent first-order kinetic fits (k_1 = 5×10^{-5} s^{-1} for both traces).

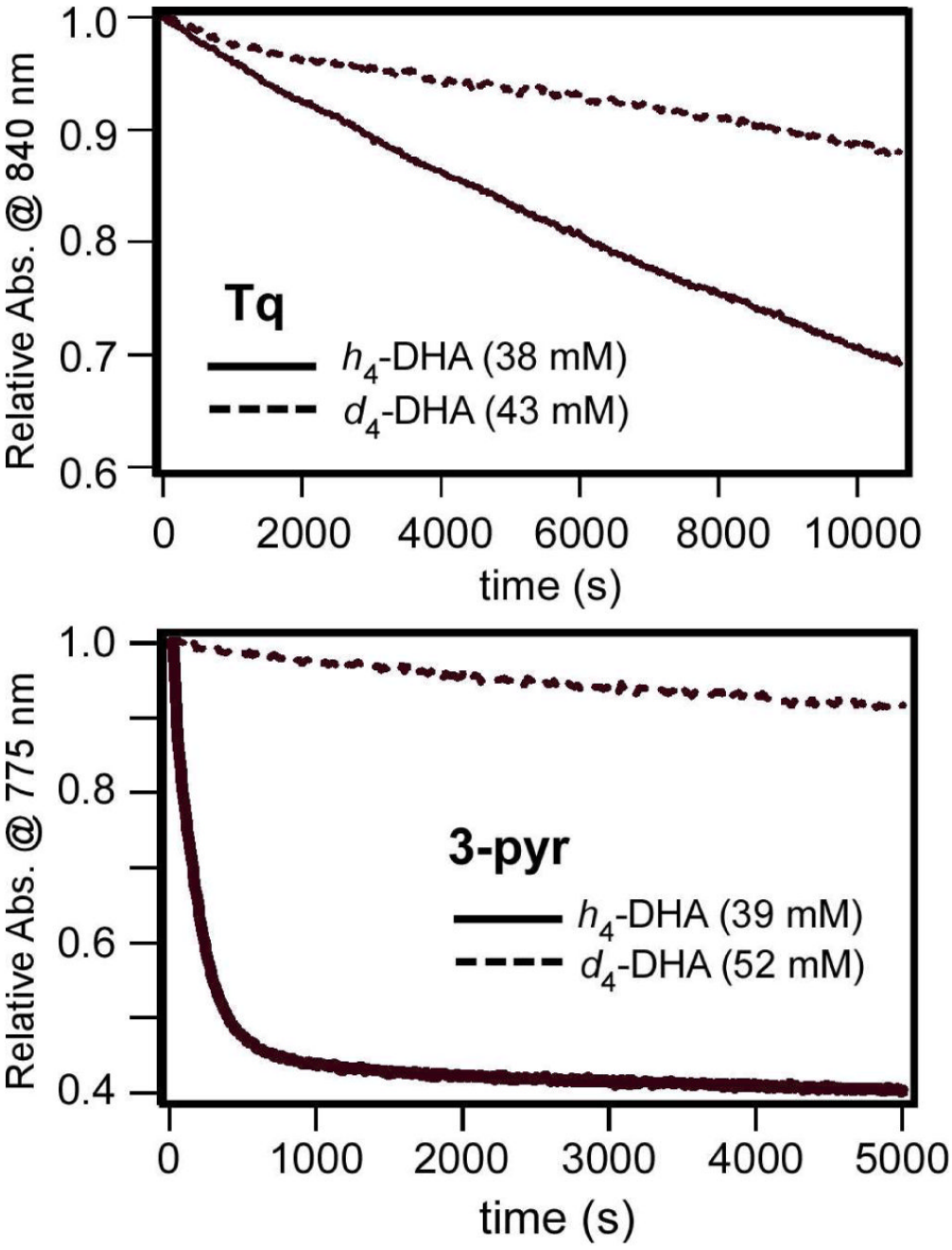

Figure 3.

Kinetic isotope effects for the reaction of **Tq** (top) and **3-pyr** (bottom) with h_4-DHA (solid lines) and d_4-DHA (dashed line) at similar concentrations. The reactions were performed in PrCN at −70 °C. Kinetic traces were measured at 840 nm for **Tq** and 775 nm for **3-pyr**, which reflect the concentration of the Fe oxidants. The traces were normalized and adjusted for minor baseline shifts. Rate constants for **Tq**: $k_1 = 4.4 \times 10^{-5}$ s^{-1} (h_4-DHA) and $k_1 = 1.1 \times 10^{-5}$ s^{-1} (d_4- DHA). For **3-pyr**: $k_1 = 5.7 \times 10^{-3}$ s^{-1} (h_4-DHA) and $k_1 = 3 \times 10^{-5}$ s^{-1} (d_4-DHA)

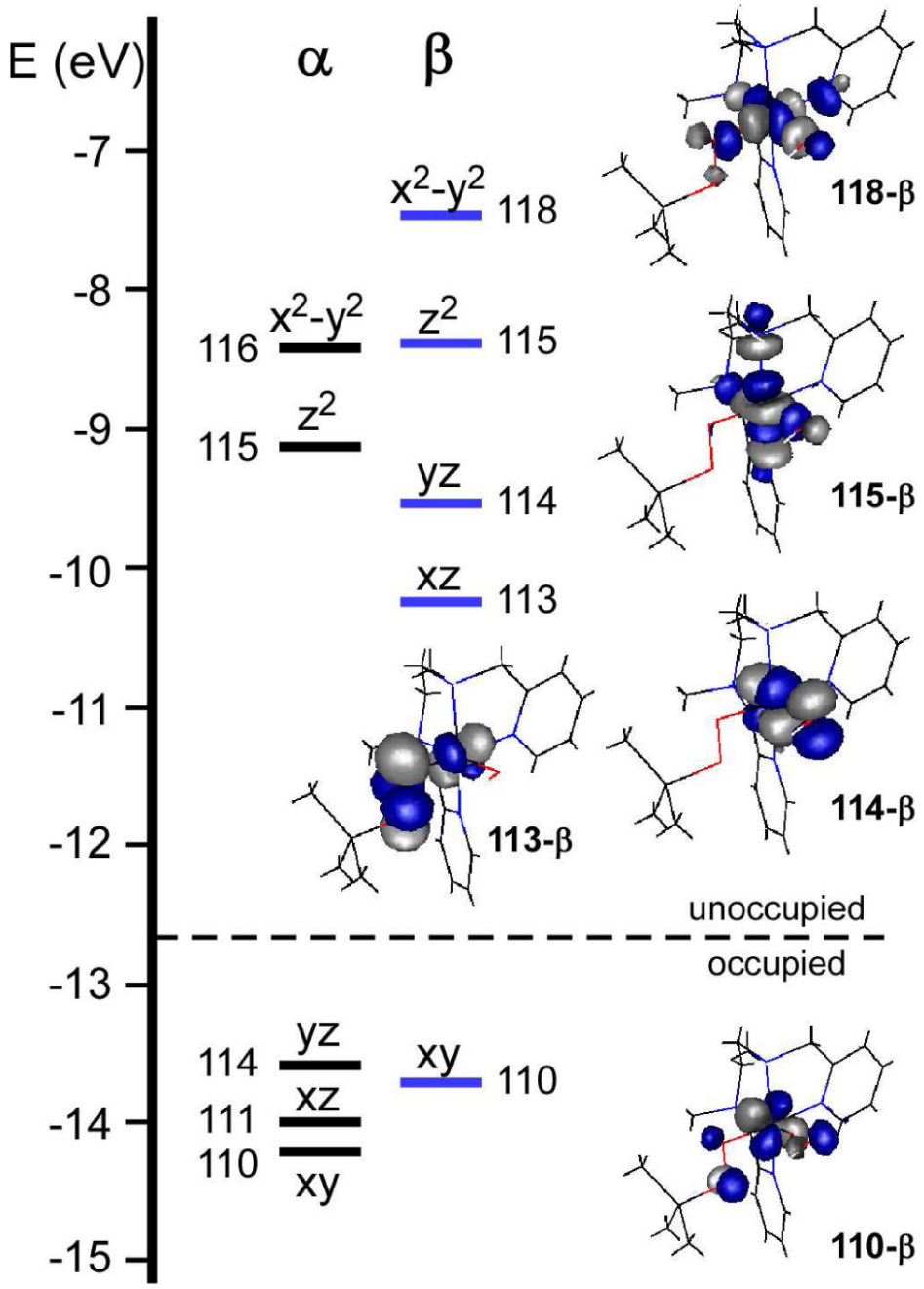

Figure 4.
Molecular orbital energy-level diagram obtained from DFT calculations on the $\mathbf{Tq^B}$ model. MOs are labeled according to their principal Fe d-orbital contributor. DFT-generated isosurface plots of the spin-down (β) Fe d-based orbitals are also shown.

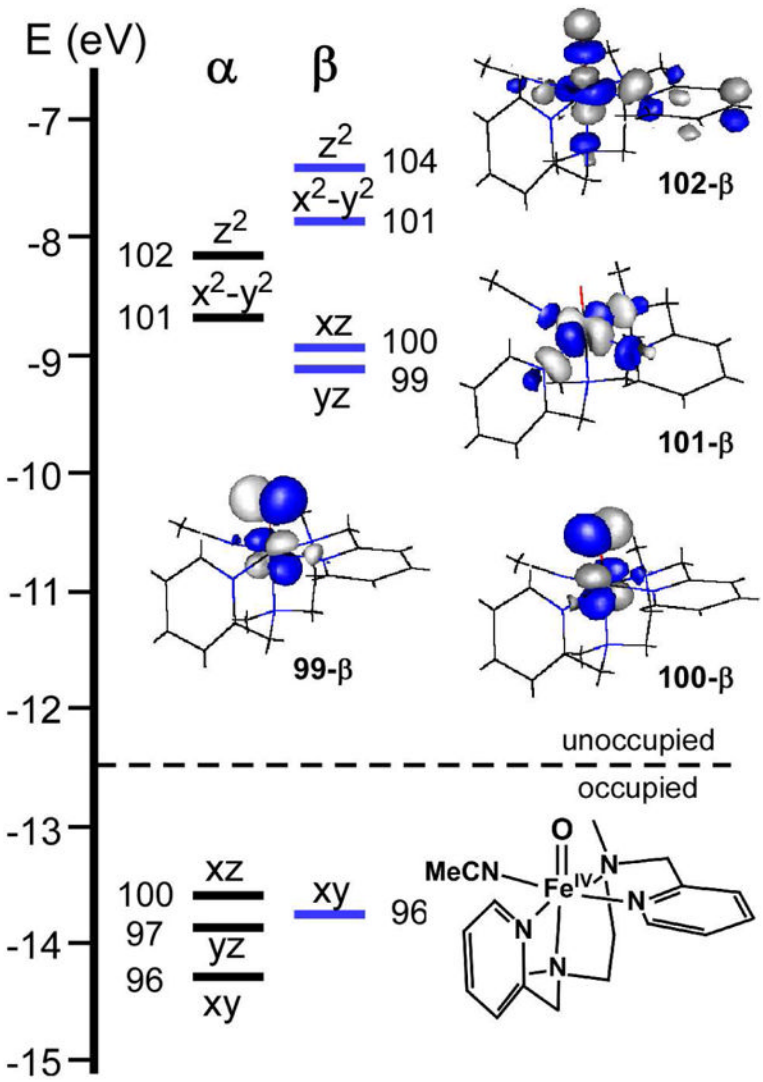

Figure 5.

Molecular orbital energy-level diagram obtained from DFT calculations on the **3^{B}NCMe** model. MOs are labeled according to their principal Fe d-orbital contributor. DFTgenerated isosurface plots of the unoccupied spin-down (β) Fe d-based orbitals are also shown.

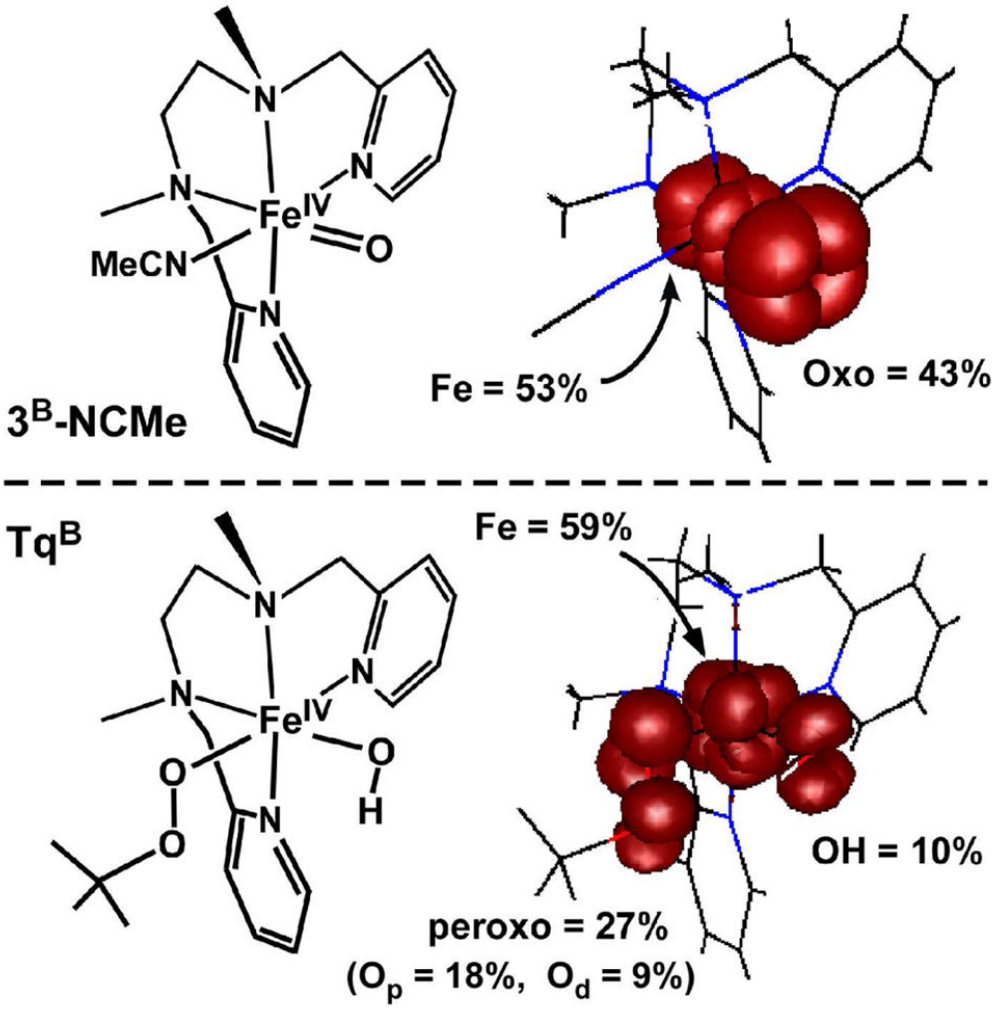

Figure 6.

DFT-generated isosurface plots representing the unpaired electronic spin-density of models **3^{B}-NCMe** (top) and **Tq^{B}** (bottom). Percentage of the total spin-density localized on specific atoms/ligands is also provided.

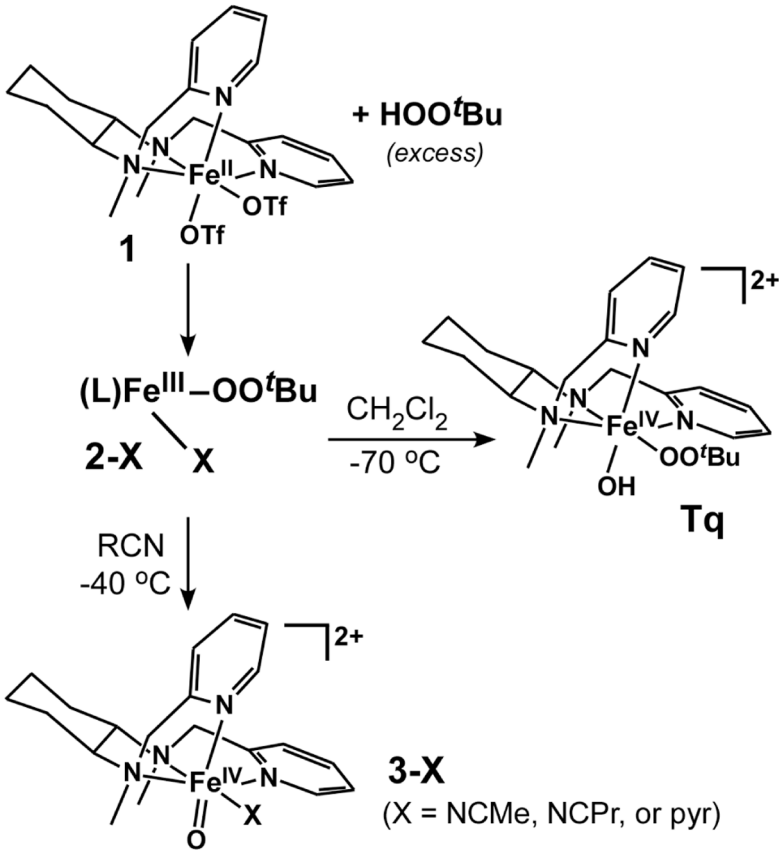

Scheme 1.

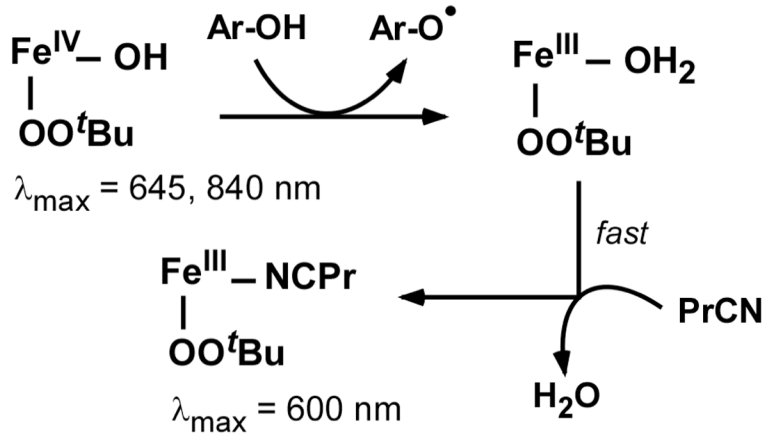

Scheme 2.

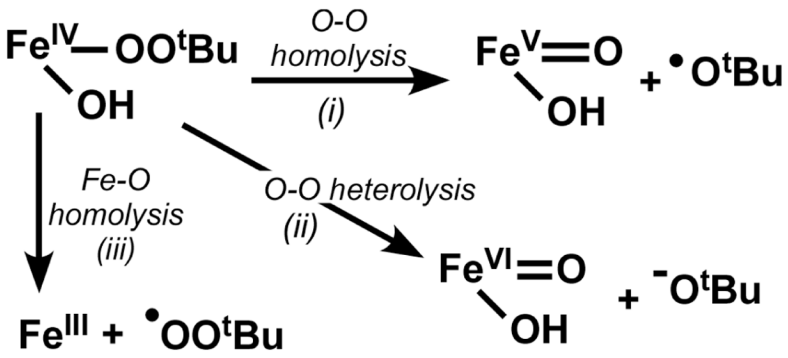

Scheme 3.

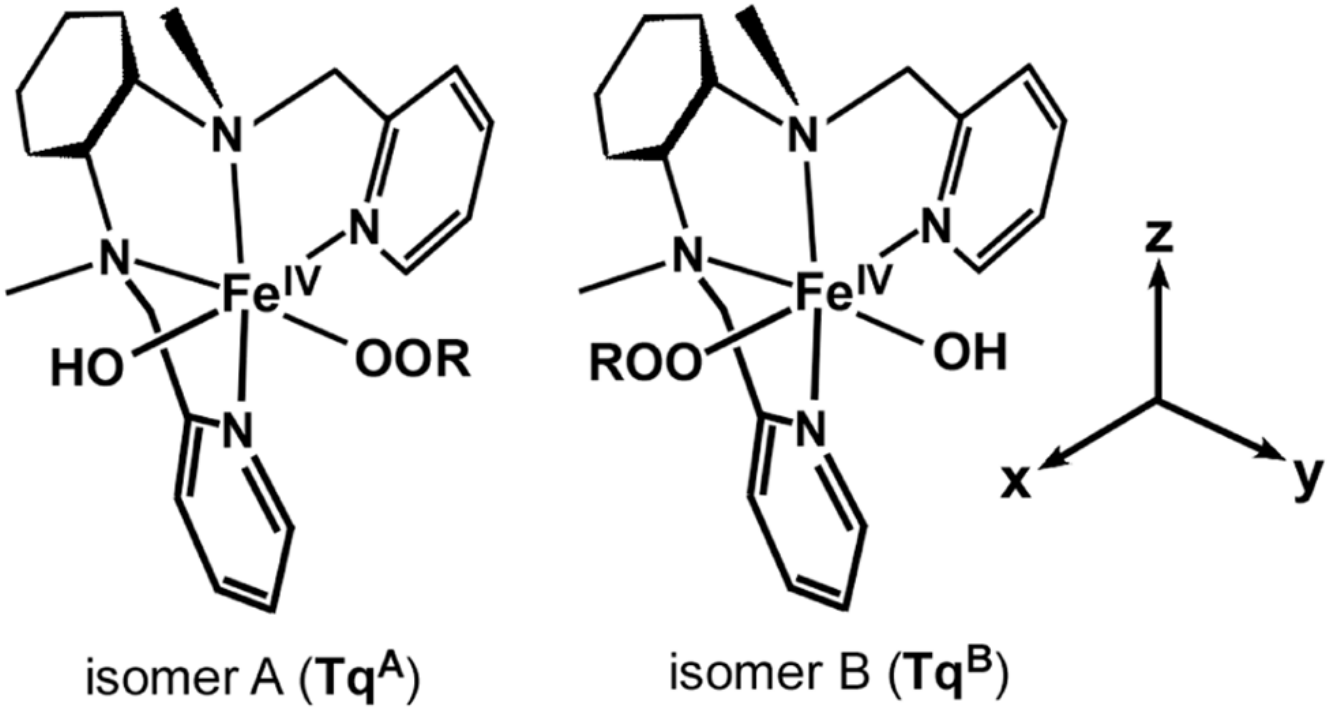

Scheme 4.

Table 1

Kinetic Parameters for the Reaction of H-atom Donors with **Tq** and **3**, and Comparison to Previously-Reported Results for Fe^{III} and Mn^{IV} Complexes.

substrate	oxidant	T (°C)	K_2 ($M^{-1}s^{-1}$)	KIE [a]	$K_2(O)/K_2(OH)$	Reference
TTBP	**Tq**	−70	$(3 \pm 1) \times 10^{-3}$	2	> 1000	*d*
	3-RCN	−70	25 ± 5	4		*d*
	3-pyr	−70	4 ± 1			*d*
	$[(PY5)Fe^{III}(OMe)]^{2+}$, *b*	25	0.60	2.0		17
DHA	**Tq**	−70	$(1.5 \pm 0.5) \times 10^{-3}$	3	100	*d*
	3-pyr	−70	0.14 ± 0.01	200		*d*
	$[(EBC)Mn^{IV}(OH)_2]^{2+}$, *c*	15	3.52×10^{-4}	3.3	43	9
	$[(EBC)Mn^{IV}(O)_2]$ *c*	15	1.50×10^{-2}	3.8		9
1,4-CHD	**Tq**	−70	$(4 \pm 1) \times 10^{-4}$		200	*d*
	3-pyr	−70	$(8 \pm 2) \times 10^{-2}$			*d*
	$[(EBC)Mn^{IV}(OH)_2]^{2+}$, *c*	15	3.64×10^{-4}		44	9
	$[(EBC)Mn^{IV}(O)_2]$ *c*	15	1.59×10^{-2}			9

[a] KIE = $k_{2,H}/k_{2,D}$

[b] PY5 = 2,6-bis(bis(2-pyridyl)methoxymethane)pyridine.

[c] EBC = 4,11-dimethyl-1,4,8,11-tetraazabicyclo[6.6.2]hexadecane.

[d] This work.

Table 2

Product Yields for the Reaction of **Tq** Solutions with Hydrocarbons at −45°C in PrCN.

substrate	atmosphere	product	Yield (equiv./Tq)	A/K ratio
cyclohexene	Ar	2-cyclohexen-1-ol	1.0 ± 0.2	2.5 ± 0.7
		2-cyclohexen-1-one	0.4 ± 0.1	
		cyclohexene oxide	trace	
cyclohexene	Air	2-cyclohexen-1-ol	1.3 ± 0.3	0.4 ± 0.1
		2-cyclohexen-1-one	3.6 ± 0.1	
		cyclohexene oxide	0.0	
adamantane[a]	Ar	1-adamantanol	0.56	2.8
		2-adamantanone	0.20	
styrene	Ar	styrene oxide	0.33 ± 0.04	N/A
		benzaldehyde	0.2 ± 0.1	
cis-stilbene	Ar	*cis*-stilbene oxide	0.09 ± 0.02	N/A
		trans-stilbene oxide	0.05 ± 0.01	

[a] Adamantane results were originally reported in reference 16.